

Improved Mechanical Properties and Corrosion Resistance of Nickel-Aluminum Bronze (NAB) Alloys by Controlling the Grain Size of Ni Coatings

Chao Feng, Yi Xie, Jun Wang, Yi Long, Wei Chen, Dengke Li, Wenbo Li, Kejian Ouyang

State Grid Hunan Electric Power Company Limited Research Institute, Changsha 410007, China;

*E-mail: 676459812@qq.com

Received: 17 March 2018 / Accepted: 13 June 2018 / Published: 5 July 2018

The surface of nickel-aluminum bronze (NAB) alloy was modified by electrodepositing Ni coating for the purpose of improving the surface mechanical and corrosion properties of the alloy. The effects of grain size (from 18 nm to 2 μm) on corrosion behaviors of Ni coatings produced by controlling the electrodeposition parameters without any grain refiner were characterized by the electrochemical workstation and the neutral salt spray (NSS) test. Transmission electron microscope (TEM) and X-ray diffraction (XRD) were used to confirm the microstructure and grain size of Ni coating. The Vickers microhardness of Ni coatings ranged between 186.70 HV to 235.325 HV, higher than that of NAB alloy (182.467 HV). The electrochemical results show that Ni coatings on NAB alloy improve corrosion resistance of the substrate alloy (NAB) and Ni coatings exhibit increasing corrosion resistance with decrease in grain size. Results of the salt spray test (The monitoring of corrosion behavior over extended periods of up to 110 days) support that Ni coatings improve the corrosion resistance of NAB substrate and the grain size of Ni coatings has a significant impact on its corrosion resistance, observed by the scanning electron microscope (SEM) coupled with energy dispersive X-ray (EDX) analyser. The experimental results can be reasonably explained by higher density grain boundaries of smaller grain size provide more nucleation sites for passive films.

Keywords: Electrodeposition, Nickel–aluminum bronze (NAB) alloys, Ni coating, Grain size, Corrosion resistance

1. INTRODUCTION

Nickel–aluminum bronze (NAB) alloys show good corrosion resistance and mechanical properties under marine conditions. Consequently, it is widely used in ship propellers, pump shafts, valve stems, valves and fittings, etc [1]. However, their widespread application is limited because of the tendency to pits, crevice, selective phase corrosion, cavitation erosion and stress corrosion

cracking under conditions of service involving exposure to seawater flowing at high speed, or with a high degree of turbulence due to the segregated composition, the coarse and loose grain sizes, and poor plasticity of NAB[2-8].

Generally, the corrosion occurs only in contact with corrosive material surface and the surface of the material structure is closely related to its corrosion resistance while it doesn't have a direct impact on the matrix organizational structure. It is known that the structure and microstructure of the surface layer of the material, directly determining the corrosion resistance of the material, can be improved effectively using surface techniques without changing the organizational structure of the matrix. Therefore, in order to reduce the maintenance requirements, expedite repair, and extend the life of the material in extreme marine condition, various surface techniques such as friction-stir process[9,10], high velocity oxygen fuel coating[11,12], laser surface melting[13,14] and electrodeposition[15] have been explored. Among them, electrodeposition has been widely used because of its advantages, especially for electrodeposited Ni and alloy coatings, which show high corrosion and wear resistance[16-18]. The advantage of electrodeposition includes 1) room temperature operation, thus reducing problems with thermal stress, 2) low equipment cost, no vacuum required; high deposition rates, 3) easy scalability. Furthermore, compared to other methods, electrodeposition is one of the most cost-effective techniques for the fabrication of nanostructured materials[19,20].

Electrodeposition of nickel (Ni) has been a major subject of electrochemists' research due to its enormous useful properties and performance characteristics[21]. Liu et al. [22] reported that the nanocrystalline (NC) Ni coatings between 10 nm and 50 nm formed compact, non-porous passive films, and the small grain size of the coating promoted the formation of compact passive film, which in turn increased the corrosion resistance in 0.5 M NaCl + 0.05 M H₂SO₄ solution. Nasirpouri et al. [21] studied the corrosion resistance of the NC Ni coatings using direct (DC), pulsed (PC), and pulsed reverse (PRC) current techniques, and the PC electrodeposited NC Ni coating with 30 nm appeared higher corrosion resistance in 2 mol/l NaOH solution. Mishra and Balasubramaniam [23] found out that NC Ni coatings (8-28 nm), which were electrodeposited using the Watt's bath with saccharine addition, formed a passive film, thus increasing the breakdown potential and improving the localized corrosion resistance. Wang's study [24] indicated the corrosion resistance of Ni coatings in alkaline solutions gradually increased with the reduction of grain size from 3 nm to 16 nm. The corrosion resistance of NC Ni is believed to be improved by the rapid formation of continuous Ni hydroxide Ni(OH)₂ passive films at surface crystalline defects and the relatively higher integrity of passive films as a result of the smooth and protective nature of the passive films formed on NC Ni coatings. Additionally, Cheng et al. [25] prepared nanocrystalline nickel coatings in sulfate solution with saccharin as additive and the study concluded that the average crystallite sizes were diminished as a result of increasing saccharin concentration and led to higher polarization resistance.

As evidenced by the literature cited above, the corrosion resistance of alloy substrates can be improved by electrodeposition of Ni and it seems to have relationship with the grain size of Ni coating. Furthermore, most of these demonstrations involved electrodeposition of Ni coating on alloy substrates, such as Mg alloy and Al alloy. However, electrodeposition of Ni coating on NAB has received only limited attention among researchers.

In this study, the primary purpose is attempted to improve the corrosion resistance of NAB through electrodeposited of Ni coating on NAB.

2. MATERIALS AND METHODS

2.1 Materials

The nickel aluminum bronze(NAB) alloy blocks used in this study was casted by vacuum melting pure Cu, Ni, Fe, Al and Mn which were purchased commercially. The nominal composition of NAB alloy blocks was gained by the fluorescence spectroscopy test, which is given in the Table 1. The specimens of NAB with a dimension of 10×10×5 mm were used as the substrates. And all the chemicals applied in the pretreatment process and electrodeposition solution were analytical reagent.

2.2 Electrodeposition of Ni coatings

Ni coatings used in this investigation were prepared by electrodeposition in the Watt's bath with pure Ni(99.99%) plate(surface area: 50cm², wrapped with a cloth) as the anode and NAB(surface area: 1cm²) as the cathode. The composition of electrodeposition solution included: Ni(SO₃NH₂)₂ · 4H₂O (350g/L), NiCl₂ · 6H₂O (15g/L), H₃BO₃(40g/L), C₁₂H₂₅-OSO₃Na (0.1g/L). The pH was adjusted at 4.0 with NH₃·H₂O and the temperature was kept at 50±5°C with a water bath. Before electrodeposition, the NAB specimens (as the substrate) were metallographically disposed by using successive grades of abrasive paper up to 1200 grit, ultrasonic cleaned with acetone for five minutes, and rinsed with deionized water for three times. In order to remove the grease on the surface, the specimens were immersed in alkaline solution consisted of NaCO₃(35g/L), NaPO₄(40g/L), NaOH(30g/L) until the appearance of a membrane on the surface, then cleaned with deionized water. For activation before electrodeposition, the specimens were dipped into H₂SO₄ (10%) solution for the membrane disappearing and rinsed with deionized water. After activation, the specimens were introduced into the Watt's bath immediately in case of oxidation. The electrodeposition parameters used in the study to obtain different grain size of Ni coating were summarized in Table 2.

Table 1. The nominal composition of NAB

Element	Cu	Al	Ni	Fe	Mn
%	81.5	9.85	3.76	3.86	1.03

Different grain sizes of Ni coatings on NAB alloy from NC to microcrystalline(MC) were produced by controlling the electrodeposition parameters using Watt's bath, without any grain refining agent.

2.3 Microstructural characterization

Transmission electron microscope (TEM) and X-ray diffraction (XRD) were used to confirm the microstructure and grain size of Ni coating. The microhardness of the samples was measured with a Vickers microhardness tester to study the mechanical properties. The microstructure and grain size of Ni coatings were directly examined by transmission electron microscope (TEM: JEM 2100F). The samples for TEM analysis were electrolyte polished by 20% perchloric acid and 80% methanol at the temperature of -30°C. The microstructures were also studied by X-ray diffraction (XRD) with a Cu-Kα target (λ=0.15405nm). The scanning 2θ was executed from 30° to 110° at the scan speed of 2°/min. The average grain sizes of the coatings were determined from X-ray peak broadening according to the Scherer equation[23]:

$$B \cos \theta = 2\varepsilon \sin \theta + 0.9\lambda / D \tag{1}$$

Where B is the full width at half maximum (FWHM) of the diffraction peaks, θ is the diffraction angle, D is the average grain size, ε is the micro-strain, and λ is the wavelength of the radiation used. The texture coefficients (TCs) for predominant (h k l) peaks were also calculated from XRD patterns, with an aim to quantify the relative crystallographic textures, which is given by Eq. (2)[26].

$$T_{hkl} = \frac{I_{hkl} / I_{hkl}^0}{\left(\frac{1}{n}\right) \sum_{h'k'l'} \left(I_{h'k'l'} / I_{h'k'l'}^0 \right)} \tag{2}$$

Where I(h k l) is the measured intensities of (h k l) peak, I⁰(h k l) is the powder diffraction intensities of Ni, and n is the number of peaks used in the calculations.

Table 2. Process parameters for electrodeposition of Ni coatings

No.	Electrodeposition parameters	
MC	Direct current (DC) electrodeposition	
	Current density	5A/dm ²
NC-1	Pulse current (PC) electrodeposition	
	Peak current density	30A/dm ²
	Pulse on-time	0.4ms
NC-2	DC	
	Current density	2A/dm ²
NC-3	Peak current density of forward pulse	2A/dm ²
	Peak current density of reverse pulse	0.5 A/dm ²
	Forward pulse on-time	5ms
	Reverse pulse on-time	5ms

2.4 Microhardness and corrosion property measurements

The microhardness of the samples was measured with a Vickers microhardness tester by performing Vickers indentations with a load force of 0.5kg and holding for 10s. And at least 5 indentations were performed for each sample to calculate the average value.

Corrosion resistance of NAB and Ni coatings were studied through electrochemical corrosion test using the electrochemical software CHI660D from China and neutral salt spray corrosion test (NSS). Before all the tests, the specimens were mechanically grounded with successive grades of abrasive papers up to 1200 grit, polished against a polishing cloth using SiC (1 μ m) sprayer until getting a mirror bright surface, ultrasonic washed with deionized water for 5 minutes and decreased with acetone.

Electrochemical corrosion tests, combined with the neutral salt spray tests (NSS) (The monitoring of corrosion behavior over extended periods of up to 110 days), were carried out to investigate the differences in corrosion behaviors among different grain size of Ni coatings and NAB observed by the scanning electron microscope (SEM) coupled with energy dispersive X-ray (EDX) analyser. The electrochemical corrosion behaviors of NAB and Ni coatings were discussed by potentiodynamic polarization and electrochemical impedance spectroscopy (EIS) in 3.5wt% NaCl aqueous solution at 30 \pm 1 $^{\circ}$ C. All the measurements were carried out in the traditional three-electrode system with the platinum electrode as auxiliary electrode, the saturated calomel electrode as reference electrode and the specimen as working electrode. The area of the working electrode exposed to the electrolyte solution was 1cm². Prior to test, the polished specimen was immersed into the 3.5wt% NaCl aqueous solution for 60 minutes to establish a stable open circuit potential (OCP). The EIS measurements were obtained at the open circuit potential in the frequency from 10KHz to 0.01Hz with the amplitude of 5mV. The equivalent circuit fitting the experimental data was analyzed by ZView software. The potentiodynamic polarization curves were received by controlling the scanning range from -0.6V to 1.0V at the scanning rate of 0.5mV/s.

In the salt spray corrosion test, the specimens were exposed the polished surface (10mm \times 10mm) to the salt mist with other faces sealed. The test was conducted according to the ASTM-B117-73 Standard Salt Spray testing with the following conditions: 1) the concentration of NaCl solution is 5wt% with the pH between 6.5 and 7.2, 2) the rate is 1~2ml/h.80cm², 3) the temperature is set at 35 $^{\circ}$ C, 4) the spray pattern is continuous. The specimens were placed in the chamber with the exposed surface upwards, and the angle of 20 $^{\circ}$ from the vertical. During the test, the observation of the specimens at fixed intervals was mainly focused on the traces of corrosion products and cracks on the bright surface. The corroded surfaces were observed by scanning electron microscope (SEM) coupled with energy dispersive X-ray (EDX) analyser.

3. RESULTS AND DISCUSSION

3.1 Microstructure and texture of Ni coatings

Surface morphology of different electrodeposited Ni coatings observed by the scanning electron microscope is shown in Fig.1. Ni coatings from Fig.1a-1c show a uniform surface morphology with refined grain size. But Ni coating electrodeposited by DC with higher current density has a non-uniform surface structure with some micro cracks in Fig. 1d. The refined grain size and the avoided micro cracks are observed in NC Ni coatings. Those evolution in surface morphology

are caused by the electrodeposition parameters, such as power supply, current density, duty ratio, frequency and so on. According to Shao[27], the higher current density obtains a higher overpotential, which decreases the activation energy of the nucleation and leads to an increased nucleation rate, resulting in a finer grain size. Besides, during the turn off pulse, the adsorbed hydrogen atoms are separated from the surface of the Ni electrodeposits, thus avoiding the progress of evolution of H_2 [28]. The nucleation mechanism from higher current density of NC-1 dominates the turn off deposition process of NC-3, and it could be the reason for the decrease in grain size for PC method (NC-1) compared to PRC method (NC-3).

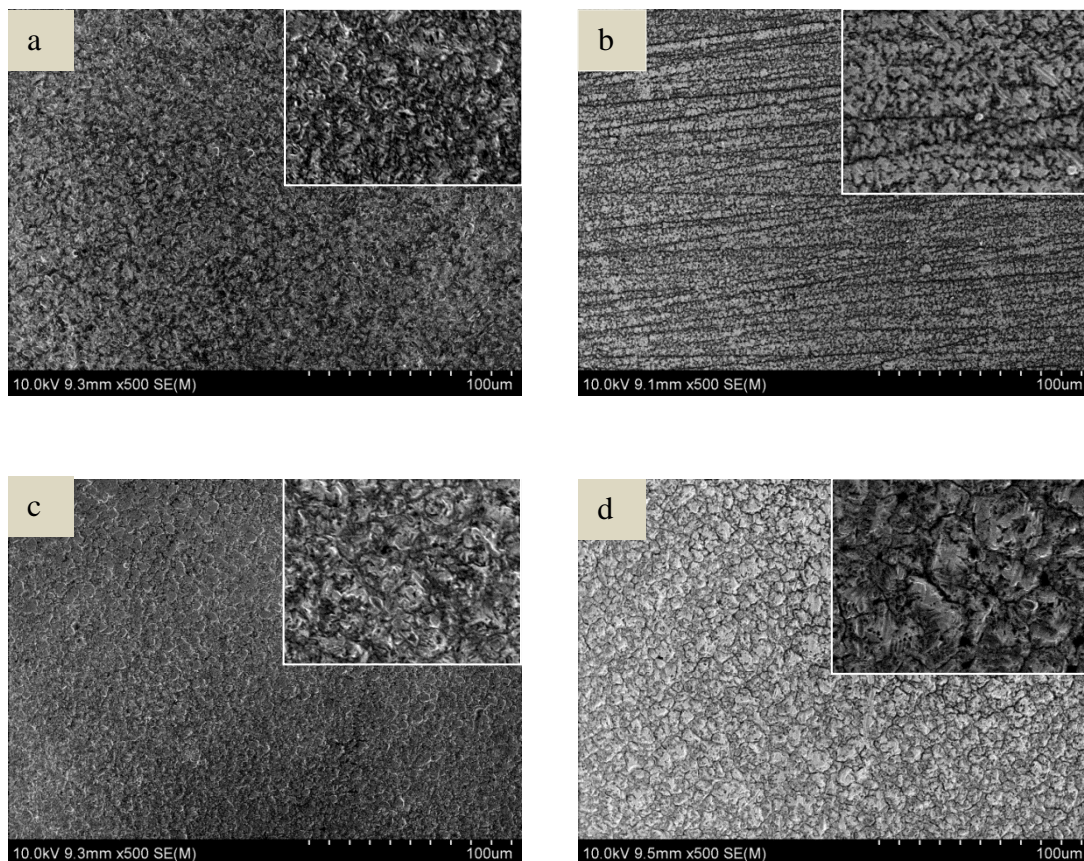


Figure 1. Surface micrographs from electrodeposited Ni coatings with different grain size: (a)NC-1; (b)NC-2; (c)NC-3; (d)MC.

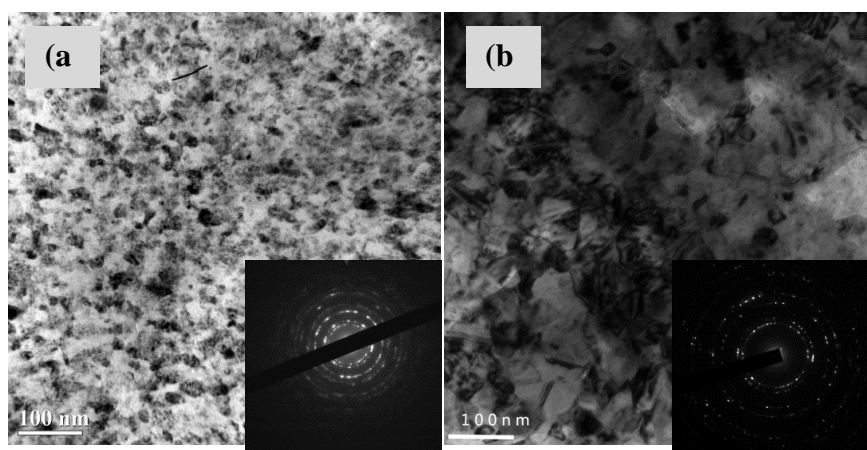
It is likely that the properties of Ni coatings respond to the changes in grain microstructure. In order to a further study of the microstructure of Ni coatings with different electrodeposition parameters, TEM and XRD measurements are applied. TEM bright field images and the corresponding selected area diffraction (SAD) patterns for the different grain sizes of Ni coatings are illustrated in Fig.2. The average grain sizes of Ni coatings with different electrodeposition parameters observed from TEM images were summarized in Table 3. For convenience, Ni coatings with different grain sizes were numbered as NC-1 for 10~20nm, NC-2 for 40~50nm, NC-3 for 150~200nm, MC for 2~3µm and pure NAB specimen as a contrast. Fig.2 shows that some regions where grain shapes and grain boundaries are clearly observed, and the grain boundary features are harder to distinguish from

other contrasts with the grain size decreasing. It is assumed that these contrasts originate mainly from microstrains and a similar observation was made by Dalla et al.[29]. In addition, SAD patterns shown in the inset of Fig.2a-2c present regular rings without additional peaks verifying a single-phase of Ni matrix with face-centered cubic crystal structure, and the first three rings of the SAD pattern correspond to the (1 1 1), (2 0 0), (2 2 0) peaks of the NC Ni coating, respectively. The SAD pattern of Fig.2d appears square spots, thus indicating polycrystalline structure of MC Ni coating.

Table 3. Summary of the observed grain sizes from TEM images.

NO.	NC-1	NC-2	NC-3	MC
Grain size (nm)	10~20	40~50	150~200	2000~3000

X-ray diffraction (XRD) patterns, illustrated in Fig.3, reveal the similar values for Ni coatings with different grain sizes according to the Scherer equation, which is not applied to the micro-grain size, shown in Table 4. As it can be seen, all the XRD patterns show the two main Bragg diffraction peaks of (1 1 1) and (2 0 0), representing that the crystallographic orientation of Ni are peaks of (1 1 1) and (2 0 0). It is clearly observed that the crystallographic structure is changed according to the intensity of (1 1 1) and (2 0 0) diffraction peaks. In Ni coatings of NC-1, NC-2, NC-3, the intensity of (2 0 0) peaks is much higher than that of (1 1 1), indicative of a preferred growth direction along with (2 0 0) crystallographic planes. However, the intensity of the peaks of MC Ni coating is relatively lower than that of the peaks of NC-1, NC-2, NC-3, which means that the MC Ni coating exhibits a random crystallographic texture[21]. The texture coefficients of Ni coatings for the observed (1 1 1) and (2 0 0) peaks are summarized in Table 5, and the texture coefficients of standard sample are the unity. For peak (2 0 0), the texture coefficients of Ni coatings are greater than that of the standard sample, which indicates a strong (2 0 0) crystallographic texture in these coatings. And the texture coefficient of (111) peak decreases obviously with the grain size increasing, suggesting that the (2 0 0) orientation gets stronger continuously.



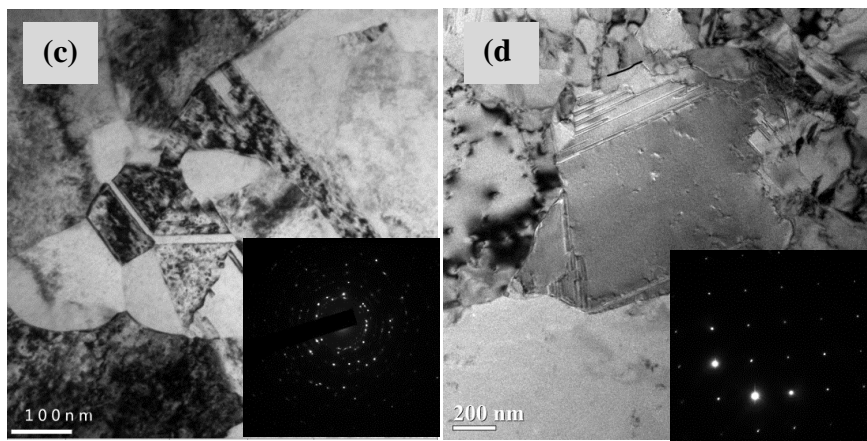


Figure 2. TEM bright field images and the corresponding selected area diffraction (SAD) patterns for Ni coatings. (a) NC-1:PC, 30A/dm²; (b) NC-2: DC, 2 A/dm²; (c) NC-3: PRC, 2 A/dm²; (d) MC: DC, 5A/dm²

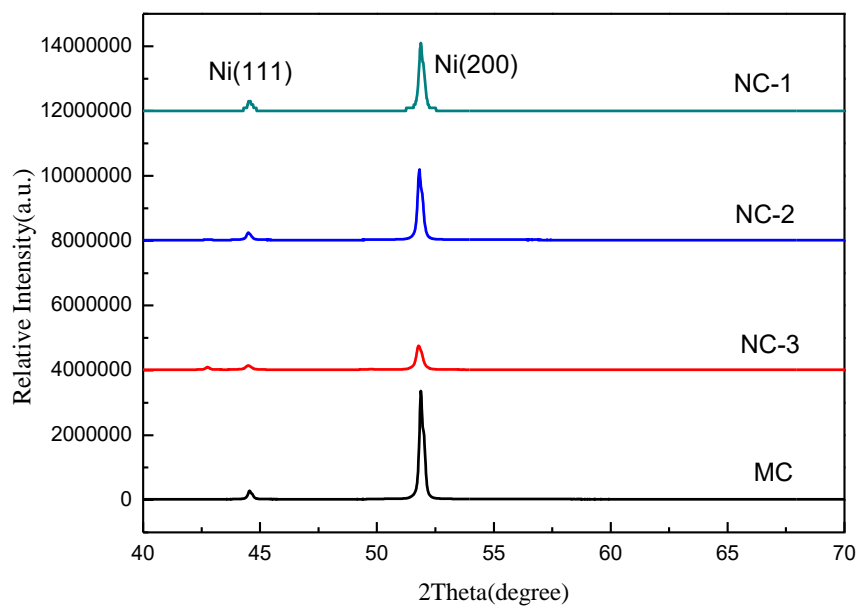


Figure 3. XRD patterns of NC Ni coatings with different grain sizes using different electrodeposition parameters: (a) NC-1, 10~20nm; (b) NC-2, 40~50nm; (c) NC-3, 150~200nm; (d) MC: 2~3μm

Table 4. Crystallite size of (1 1 1) and (2 0 0) planes calculated for Ni coatings with different grain size from XRD spectrum.

	Grain size (nm)		
	Peak/2θ		Average
	(1 1 1)/44°	(2 0 0)/52°	
NC-1	23.39	24.62	24.01
NC-2	42.79	38.94	40.87
NC-3	137.30	133.12	135.21

Table 5. Texture coefficients (TCs) of various (h k l) planes for standard sample, and different grain size Ni coatings.

Sample	Texture coefficient (TC)	
	(1 1 1)	(2 0 0)
Standard Sample	1	1
NC-1	0.305	1.695
NC-2	0.178	1.822
NC-3	0.168	1.832
MC	0.139	1.861

3.2 Mechanical strength

The variation of vickers hardness of NAB and Ni coatings are presented in Fig.4. Hardness obtained from the polished surface of Ni coatings show a substantial increase compared to the NAB, which represents an improvement in the surface properties. Generally, microhardness is influenced by the grain size, internal stress and the cavities. Thus, onereason for increasing hardness value of Ni coatings is possibly due to the smaller grain size of Ni coatings than that of NAB alloy. In addition, the microhardness of NC-1 coating (10~20nm) is almost 20% higher than that of MC coating (2~3um), and the microhardness increases with decreasing of grain size. It is assumed that this phenomenon is mainly owing to the high density of grain boundaries, which impede the movement of dislocation and deformation of the materials.

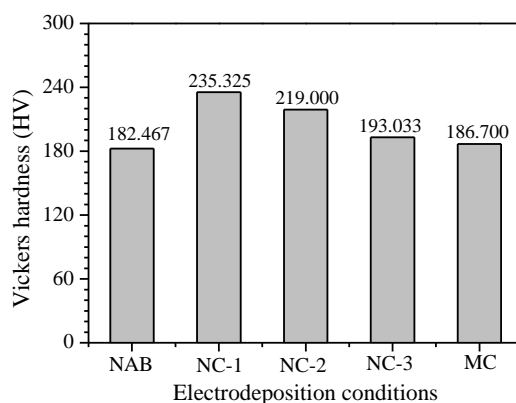


Figure 4. Vickers hardness of NAB and Ni coatings with different grain sizes.

3.3 Electrochemical corrosion

The experiments for electrochemical properties of NAB and Ni coating are carried out in 3.5wt% aqueous NaCl solution and the potentiodynamic polarization curves are illustrated in Fig.5. It can be seen from the figure that the corrosion resistance of Ni sample is higher than NAB sample and it means that our idea is feasible. The objectives are to discuss the effects of grain size on mechanical and corrosion behaviors of Ni coatings.

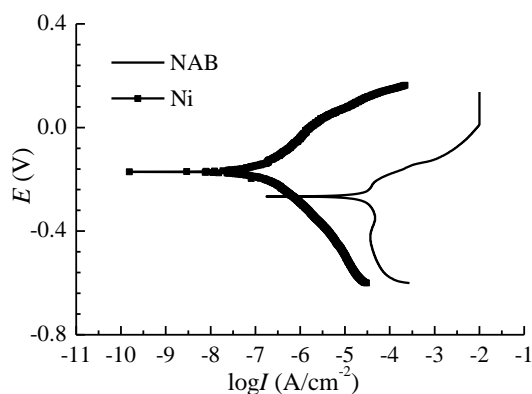


Figure 5. Potentiodynamic polarization curves of NAB and Ni samples in aerated 3.5% NaCl solution.

Typical potentiodynamic polarization curves of NAB and Ni coatings with different grain sizes carried out in 3.5 wt% NaCl aqueous solution are shown in Fig.6. The Ni coatings show a typical active-passive behavior. The stage of passivation, associated with the formation of passive films, is one of the factors that improve the corrosion resistance in 3.5 wt% NaCl aqueous solution. It was considered that the passivation involved the hydrolysis reaction, according to the following reactions[24]:



Normally, the passive films cover over the surface of the corroded samples, thus providing a barrier between electrolyte solution and electrode. It is increasing the difficulty for further electrochemical reaction, thus creating the passivation region.

In general, the corrosion potential and corrosion current density are used to determine the active corrosion ability of materials. As seen from Fig.6, the corrosion potentials of the Ni coatings are shifted towards more positive compared to the pure NAB alloy, which means NAB is much more prone to corrosion in 3.5 wt% NaCl aqueous solution as a result of the soluble CuCl_2^- species formed on the surface, which promote the active region of Cu-alloy to be attacked by chloride ion, thus leading to the dissolution of Cu in the alloy[30].

The polarization resistance R_p was calculated from the Stern-Geary formula [17]:

$$R_p = \left(\frac{dE}{di} \right)_{i \rightarrow 0} = \frac{\beta_a \beta_c}{2.303(\beta_a + \beta_c)} \times \frac{1}{i_{\text{corr}}} \quad (6)$$

Where β_a and β_c are the anodic polarization slope and cathodic polarization slope, i_{corr} is the corrosion current density. The corrosion potential (E_{corr}) and corrosion current density (i_{corr}) are calculated from the polarization curves by extrapolation. The results were summarized in Table 6. It clearly reveals that the value of corrosion current density of Ni coatings is sharply decreased and polarization resistance significantly increases with the reduction of the grain size. The observation indicates that the corrosion resistance of Ni coating is closely related to the grain size. Moreover, ultrafine Ni coating (10~20nm) possesses dozens of times lower corrosion current density (about $1.6760\text{E}^{-6}\text{A/cm}^2$) than that of MC Ni coating (about $66.7\text{E}^{-6}\text{A/cm}^2$). The reason for this phenomenon is

because of the higher density of grain boundaries and intergranular dislocations with smaller grain size, where the sites for passive films are easier to nucleated[31]. Therefore, it can be deduced that corrosion resistance of Ni coatings in NaCl aqueous solution were greatly enhanced by the reduction of grain size because of the tense nucleation sites for passive films.

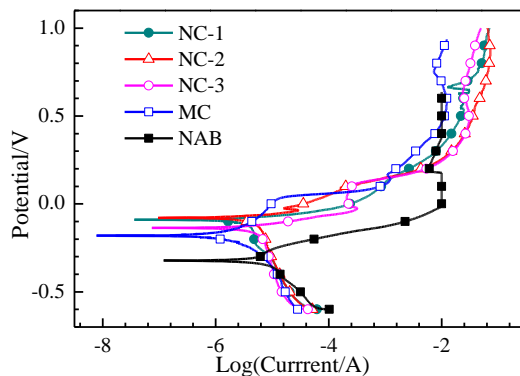


Figure 6. Polarization curves of nickel of different grain sizes in 3.5 wt.% NaCl solution

Table 6. Results from Tafel curves of E_{corr} , i_{corr} , β_α , β_c and R_p with different grain sizes and nickel-aluminum bronze.

Samples	i_{corr} (A/cm ²)	E_{corr} (mV)	β_α (mV/decade)	β_c (mV/decade)	R_p (kΩ/cm ²)
NC-1	1.67E-6	-88	9.38	0.23	58.90
NC-2	9.71E-6	-78	10.10	1.47	57.45
NC-3	12.32E-6	-135	12.92	1.15	37.29
MC	66.70E-6	-178	4.73	4.68	15.30
NAB	9.77E-6	-320	12.65	2.83	102.72

In order to confirm the polarization results, the Nyquist impedance plots of NAB and Ni coatings in 3.5 wt% NaCl aqueous solution are shown in Fig.7. All the Nyquist plots exhibit a capacitance loop with different diameters in the frequency range. Fig.6 shows that the diameters of the capacitance loop of Ni coatings are clearly larger than that of NAB, indicating the higher corrosion resistance of Ni coatings. By analyzing the Nyquist plots, it can be easily identified that the diameters of Ni coatings at higher frequency depend remarkably upon the grain size. According to the magnification in high frequency, the maximum and minimum diameter of Ni coatings are achieved for grain size of 10~20 nm and 2~3 μm, respectively. Generally, the corrosion resistance is usually estimated by the diameter of the Nyquist plots. This means that the corrosion resistance of Ni coating increases in turn with grain size in descending order. In order to simulate the corrosion reaction in 3.5 wt% NaCl aqueous solution, an equivalent electrical circuit (shown in the inset of Fig.7) was proposed to fit the impedance spectra of Ni coatings and NAB, which consists of solution resistance (R_s), film resistance (R_f) and film constant phase (CPE). CPE is often used instead of a capacitor to compensate for inherent inhomogeneity in the system and defined by two parameters (T and P), which are independent of frequency [21]. In addition, the impedance at the solution/electrode interface was

provided by the formation of Ni(OH)₂ passive films. The results derived from fitting the Nyquist plots are presented in Table 7. The mean error of modulus in this table is less than 4%, implying a good fitting between the experimental data and the equivalent electrical circuit. By analyzing the data in this table, grain size of Ni coating has a great link to the corrosion resistance in the NaCl aqueous solution. The film resistance increased with the decreased grain size of Ni coatings, many times higher than that of NAB. This claims a clear indication that corrosion resistance of Ni coating is increased with the decreasing grain size. In this case, higher density grain boundaries of smaller grain size provide more nucleation sites for passive films, according to the similar research of Wang et al.[23].

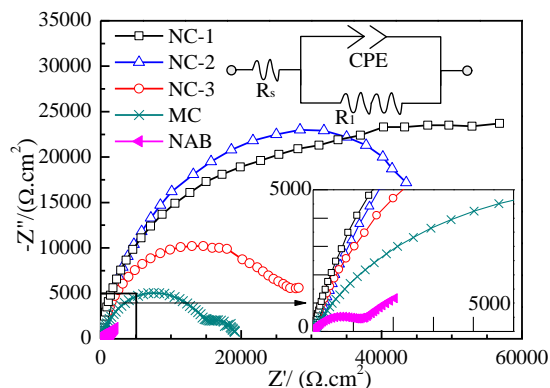


Figure 7. Nyquist impedance diagrams for nickel coatings and nickel-aluminum bronze in 3.5 wt% NaCl solution

Table 7. The equivalent circuit parameters determined by fitting the impedance spectra of NAB alloy and Ni coatings with different grain sizes in 3.5 wt% NaCl aqueous solution

Element	Rs(Ωcm ⁻²)	R ₁ (kΩcm ⁻²)	CPE-T(Fcm ⁻² s ^{p-1})	CPE-P	Error (%)
NC-1	14.8	59.2	6.53E-5	0.83	1.12
NC-2	8.5	56.0	2.70E-5	0.88	1.26
NC-3	8.8	26.6	3.57E-5	0.88	2.06
MC	26.2	17.0	2.14E-6	0.76	3.63
NAB	6.2	1.9	3.07E-4	0.73	2.94

3.4 Salt spray corrosion test

The surface morphologies of all specimens in the salt spray chamber for 9 days are shown in Fig.8. The green corrosion products were first emerged on the surface of NAB alloy after 1 day in the salt spray chamber, and the green corrosion products accumulated on the surface with time extension. However, the red rust on Ni coatings with different grain size showed different degrees of corrosion resistance. As is shown in Fig.8, it is clearly observed that the area ratio of the red rust increases with the grain size increasing, meaning that the corrosion resistance decreases with grain size increasing. This phenomenon merely confirms that the NAB substrate corrodes much more easily compared to Ni coating in neutral NaCl solution.

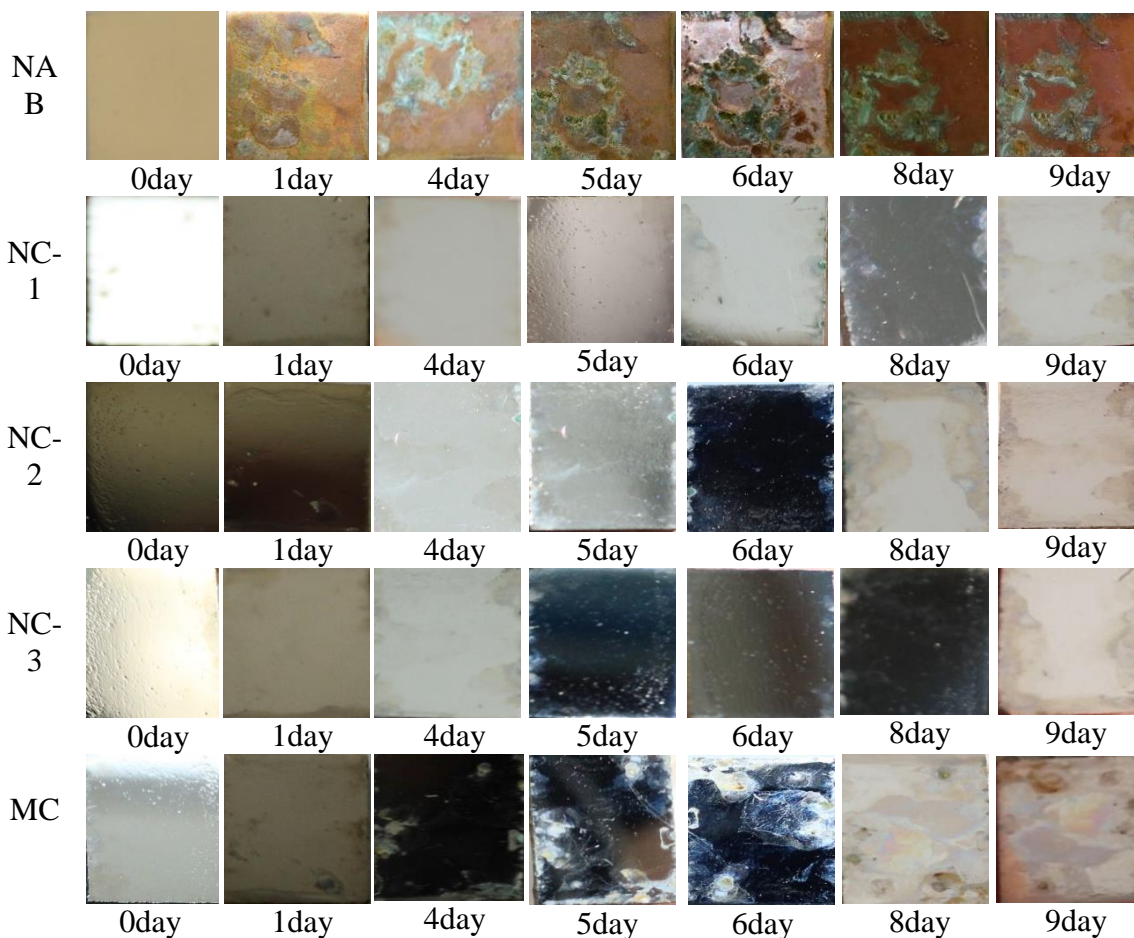


Figure 8.The surface macroscopic morphology of NAB alloy and nickel coatings in the salt spray test with different time.

And this behavior is possibly attributed to the continuous and compact passive films formed on the surface of Ni coatings.

After tested in the salt spray chamber for 110 days, none of the Ni coatings demonstrated visible trace of corrosion process. Scanning electron microscope (SEM) has been used to observe the corroded surfaces of Ni coatings. The morphologies of the Ni coatings are shown in Fig.8. As Fig. 9 shows, the surface of Ni coatings appeared cracks and corrosion products, which were analyzed by EDS microanalyses shown in Fig.10. In NaCl aqueous solution, Ni coatings were attacked by chloride ions which adsorbed the intermediate species to form insolubility, thus hindering the formation of the passive film and leading to the local metal dissolution[33]. Fig.10 shows Cl and Cu in the corrosion products, revealing that Cl had penetrated into the substrate through some corroded voids because of the Cl attacking the passivation film as corrosive medium[32]. The products occupied on the surface and spread in manner of compact flows, which gave the appearance of cracks because of the dehydration of the surface corrosion products[33]. By comparing the results from Fig.9, grain size of the coating has a great effect on the corrosion surface morphology, such as corrosion products and cracks. It is obviously observed that corrosion products become much less with the grain size

becoming smaller. Besides, the intensity of cracks decreased and depth became shallow with the reduction of grain size. This means that corrosion resistance of Ni coatings in NaCl spray test increase with the grain size decreasing. And this increasing behavior is caused mainly due to the passive films formed on the surface, which is consistent with the electrochemical testing results.

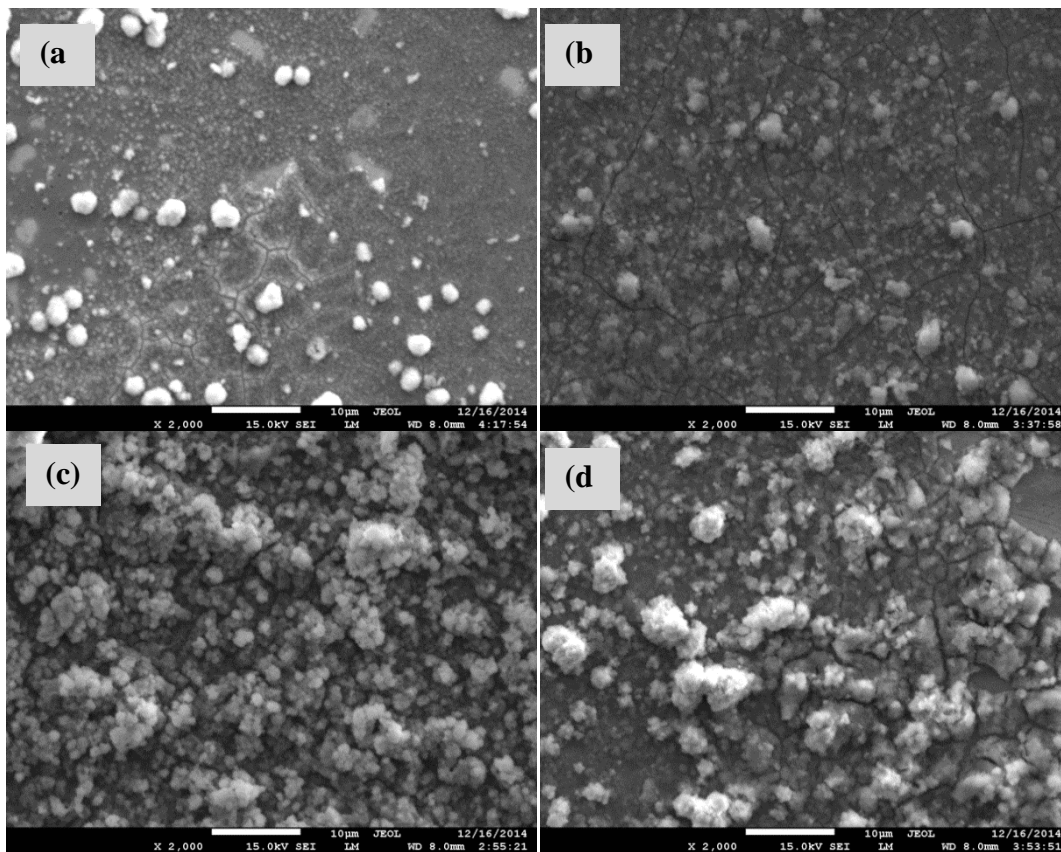


Figure 9. Corrode morphologies of NAB alloys with nickel coatings with different grain sizes in the salt spray test for 9 days: (a) NC-1; (b) NC-2; (c) NC-3; (d) MC.

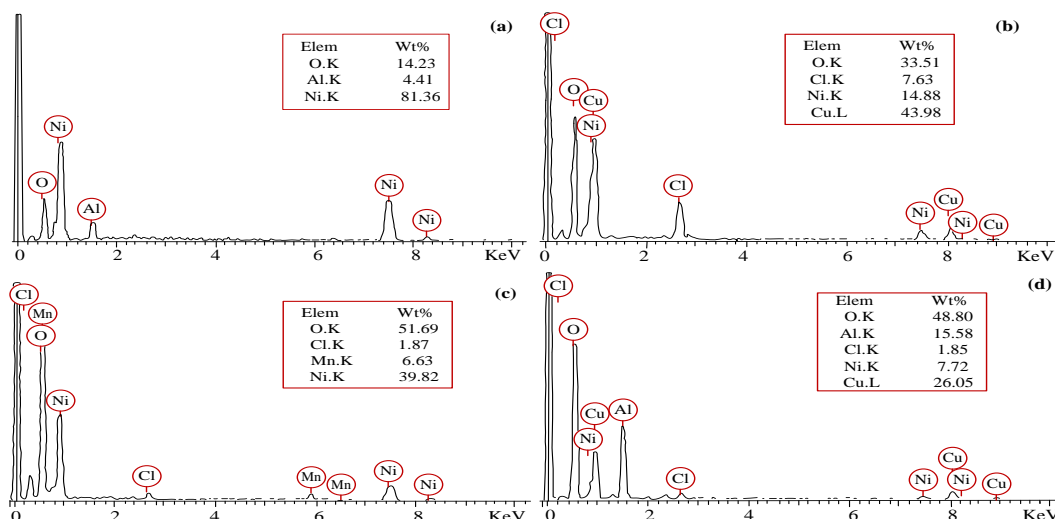


Figure 10. EDS analysis of corrosion products of NAB alloys with nickel coatings with different grain sizes in the salt spray test for 9 days: (a) NC-1; (b) NC-2; (c) NC-3; (d) MC.

4. CONCLUSIONS

Different grain sizes of Ni coatings on NAB alloy were produced by controlling the electrodeposition parameters. All the coatings had higher hardness and corrosion resistance compared to the substrate NAB alloy because of the passive films formed on the surface of Ni coating in 3.5 wt% NaCl aqueous solution. The effect of grain size of Ni coating on corrosion resistance has also been discussed. Electrochemical results showed that corrosion current density decreased and the film resistance increased with the reduction of grain size, owing to the higher nucleating sites for more passive films with smaller grain size. The corrosion behaviors obtained by the salt spray test revealed the corrosion mechanism that chloride ions attacked the Ni coatings to enhance dissolubility thus hindering the formation of passive films and leading to the corrosion process.

References

1. C.X. Hong, C.H. Jiang, Z. Chai, M. Chen, L.B. Wang and V. Ji, *Surf. Coat. Tech.*, 313 (2017) 136.
2. B.B. Zhang, J.Z. Wang, J.Y. Yuan and F.Y. Yan, *Mater. Corros.*, 1 (2018) 69.
3. Y. Lv, L. Wang, J. Mao and W. Lu, *Rare Metal Mat. Eng.*, 53 (2018) 2463.
4. P. Linhardt, S. Kühner, G. Balland M.V. Biezma, *T. Nonferr. Metal. Soc.*, 26 (2016) 1105.
5. Q. Luo, Z. Wu, Z. Qin, L. Liu and W.B. Hu, *Surf. Coat. Tech.*, 309 (2017) 106.
6. X.R. Feng, X.F. Cui, G. Jin, W. Zheng, X. Wen, Z.B. Cai, X. Wen, B.W. Lu and J.M. Liu, *Surf. Coat. Tech.*, 333 (2018) 104.
7. H.N. Krogstad, R. Johnsen, *Corros. Sci.*, 121 (2017) 43.
8. S. Thapliyal, D.K. Dwivedi, *J. Mater. Process. Tech.*, 238 (2016) 30.
9. B. Zhang, J. Wang and F. Yan, *Corros. Sci.*, 131 (2018) 252.
10. W.Z. Zhai, W.L. Lu, P. Zhang, J. Wang, X.J. Liu and L.P. Zhou, *Appl. Surf. Sci.*, 436 (2018) 1038.
11. S.S. Bang, Y.C. Park, J.W. Lee, S.K. Hyun T.B. Kim, J.K. Lee, J.W. Han and T.K. Jung, *J. Nanosci. Nanotechnol.*, 18 (2018) 1931.
12. L.L. Silveira, G.B. Sucharski and A.G.M. Pukasiewicz, *J. Therm. Spray Techn.*, 1-2 (2018) 1.
13. C.H. Tang, F.T. Chen and H.C. Man, *Mater. Sci. Eng. A*, 373 (2004) 195.
14. C.H. Tang, F.T. Chen and H.C. Man, *Surf. Coat. Tech.*, 182 (2004) 300.
15. C.A. Huang, T.H. Wang, T. Weirich and V. Neubert, *Corros. Sci.*, 50 (2008) 1385.
16. X. Guo, S. Wang, J. Gong, J. Guo, L. Peng and W. Ding, *Appl. Surf. Sci.*, 313 (2014) 711.
17. H. Yang, X. Guo, X. Chen and N. Birbilis, *Corros. Sci.*, 79 (2014) 41.
18. S.H. Mosavat, M.H. Shariat, M.E. Bahrololoom, *Corros. Sci.*, 59 (2012) 81.
19. G.J. Snyder, J.R. Lim, C.K. Huang J.P. Fleurial, *Nat. Mater.*, 8 (2003) 528.
20. F. Xiao, C. Hangarter, B.Y. Yoo, Y.W. Rheem, K.H. Lee and N.V. Myung, *Electrochim. Acta*, 52 (2008) 8103.
21. F. Nasirpouri, M.R. Sanaeian, A.S. Samardak, E.V. Sukovatitsina, A.V. Ognev, L.A. Chebotkevich, M.G. Hosseini and M. Abdolmaleki, *Appl. Surf. Sci.*, 292 (2014) 795.
22. L. Liu, Y. Li and F. Wang, *Electrochim. Acta*, 53 (2008) 2453.
23. R. Mishra, R. Balasubramaniam, *Corros. Sci.*, 46 (2004) 3019.
24. L. Wang, J. Zhang, Y. Gao, Q. Xue, L. Hu and T. Xu, *Scripta Mater.*, 55 (2006) 657.
25. W. Cheng, W. Ge, Q. Yang and X. Qu, *Appl. Surf. Sci.*, 276 (2013) 604.
26. Y.Q. Wang, T. Wu and Z. Lan, *J. Mater. Sci. Tech.*, 31 (2015) 175.
27. L.G. Wang, L.Q. Du and L.D. Wang, *Micro Nano Lett.*, 5 (2010) 165.
28. M. Motoyama, Y. Fukunaka, T. Sakka, Y.H. Ogata and S. Kikuchi, *J. Electroanal. Chem.*, 584 (2005) 84.

29. T.F. Dalla, S.H. Van and M. Victoriab, *Acta Mater.*, 50(2002) 3957.
30. K.M. Ismail, A.M.Fathi and W.A. Badawy, *Corros. Sci.*,48(2006) 1912.
31. Z.R. Wang, K.T. Aust and U. Erb, *Acta. Metallur. Mater.*,43(1995) 519.
32. C. Xu, L. Du, B. Yang and W. Zhang, *Surf. Coat. Tech.*,205(2011) 4154.
33. Y. Ma, Y. Li and F. Wang, *Corros. Sci.*,51(2009) 997.

© 2018 The Authors. Published by ESG (www.electrochemsci.org). This article is an open access article distributed under the terms and conditions of the Creative Commons Attribution license (<http://creativecommons.org/licenses/by/4.0/>).